Clay Minerals, (2018) **53**, 665–674

Microstructural and porosimetry analysis of Ag-TiO_2 intercalated kaolin and diatomite as nanocomposite ceramic materials

EMMANUEL AJENIFUJA[1,2,*], ABIMBOLA P.I. POPOOLA[1], KABIR O. OYEDOTUN[3] AND OLAWALE POPOOLA[2]

[1] *Department of Chemical, Metallurgical and Materials Engineering, Tshwane University of Technology, Pretoria, South Africa*
[2] *Center for Energy and Electric Power, Tshwane University of Technology, Pretoria, South Africa*
[3] *Department of Physics and Engineering Physics, Obafemi Awolowo University, Ile-Ife, Nigeria*

(*Received 4 April 2018; revised 26 August 2018; Accepted Manuscript published online: 17 December 2018; Version of Record published online: 22 January 2019; Associate Editor: M. Pospišil*)

ABSTRACT: Kaolin and diatomite are abundant and widely available geological materials that may immobilize or stabilize functional chemical species on their surfaces for various applications. Acid-treated kaolin and diatomite were intercalated with photocatalyst Ag-TiO_2 nanoparticles using the sol–gel technique to prepare nanocomposite ceramic materials. The nanocomposites were sintered between 900°C and 1000°C to induce thermal reactions and to enhance nanoparticle–substrate attachment. Chemical and thermal characterizations of the acid-treated materials and intercalated nanocomposites were performed with energy-dispersive X-ray (EDX) analysis and differential scanning calorimetry (DSC), respectively. The Brunauer–Emmett–Teller (BET)-specific surface area and scanning electron microscopy (SEM) were employed for physical and microstructural characterization of the nanocomposites, respectively. Morphological studies revealed a uniform distribution of Ag-TiO_2 nanocrystallites in pores and on mineral particle surfaces. The BET analysis showed remarkable surface and grain modification by sintering. Decreases in the BET-specific surface area were observed for the sintered ceramic nanocomposite, Ag-TiO_2-kaolin (20.244 to 5.446 m^2/g) and Ag-TiO_2-diatomite (19.582 to 10.148 m^2/g).

KEYWORDS: kaolin, diatomite, BET-specific surface area, sol–gel, ceramics, adsorbents.

The combination of natural mineral matrices and chemical compounds often leads to products with interesting and unique properties (Gomez-Romero & Sanchez, 2004; Ruiz-Hitzky & Van Meerbek, 2006). From a physicochemical point of view, this process permits the formation of bi- or multi-functional materials, combining the chemical and physical properties of the two end-members (Alexandre & Dubois, 2000; Pinnavaia & Beall, 2000; Ray & Okamoto, 2003; Carrado, 2004). This combination often leads to the modification of the physicochemical properties of the support mineral, such as the specific surface area, adsorption, hydrophobicity, *etc*. Functional chemical species may be immobilized and stabilized on suitable substrates or layers. Among the nanohybrid materials, clay–photocatalyst composites are promising due, in particular, to the broad availability of natural clay minerals and their ability to incorporate a large variety of functional molecules on their surfaces (Tunney & Detellier, 1996; Elbokl & Detellier, 2006, 2009; Fernandez-Saavedra *et al.*, 2008; Letaief *et al.*, 2008; Defontaine *et al.*, 2010).

*E-mail: ajenifujae@tut.ac.za
https://doi.org/10.1180/clm.2018.50

Kaolin and diatomite are widely available geological materials that have been used for decades in their natural forms domestically and for environmental remediation issues. They are also applied in agriculture as natural insecticides, food protectants, cosmetics and paints (Fields *et al.*, 2002; Faulde *et al.*, 2006; Ferraz *et al.*, 2011; Leiviskä *et al.*, 2012). Due to strong interactions between the tetrahedral and the octahedral sheets through H-bonds and dipolar interactions in kaolinite, the main mineral of kaolins, direct intercalation of functional compounds into the kaolinite interlayer is rarely reported. Natural diatomite has a weak adsorption capacity because of its macrostructure. However, the SiO_2 materials and clay minerals may be chemically activated to modify and enhance their adsorption capacity *via* increases in porosity and surface activity tuning for improved adsorbent–adsorbate interactions (Mokaya *et al.*, 1993; Vicente Rodriguez *et al.*, 1994; Komadel, 1999; Ozcan & Ozcan, 2004; Bergaya *et al.*, 2006; Plachá *et al.*, 2008, 2014). TiO_2 is widely used for its photocatalytic properties, being more active in the ultraviolet region. Though it is considered a non-toxic material (Warheit *et al.*, 2007; Jiang *et al.*, 2009), the possibility of it being biohazardous has still not been ruled out completely (Li *et al.*, 2008). Therefore, direct utilization and discharge of TiO_2 nanoparticles (NPs) and other photocatalysts into the environment should be discouraged. The most affordable and easiest way to achieve this is to anchor and secure TiO_2 NP photocatalysts on the surface of a suitable substrate (Wang *et al.*, 2009; Vimonses *et al.*, 2010). Aluminosilicates are cheap and abundant materials with unique physicochemical properties that characterize an excellent substrate for anchoring metal oxide NPs (Szabó *et al.*, 2003; Wang *et al.*, 2009; Vimonses *et al.*, 2010). Recently, kaolin and diatomite were intercalated with Ag-TiO_2 NPs, and the prepared photocatalyst nanocomposites exhibited enhanced functionalities for degradation and adsorption of pollutants (Cu^{2+} and Co^{2+}) from high-concentration (100–1000 mg/L) aqueous solutions (Chong *et al.*, 2014; Ajenifuja *et al.*, 2017a, 2017b). The use and control of mineral–photocatalyst NPs is easier than that of pure photocatalyst NPs, because their ceramic nature gives the nanocomposite its required physical integrity when in contact with pollutants (Burg *et al.*, 2007; Hathway & Jenks, 2008; Wang *et al.*, 2009). More information on the physical and chemical characterizations of photocatalyst–silica or aluminosilicate mineral ceramic nanocomposites is still necessary. In this study, kaolin and diatomite were modified with photocatalytic AgNP-TiO_2 NPs *via* the sol–gel process and subsequent high-temperature sintering. Microstructural and thermal characterization of the ceramic nanocomposites were carried out, while porosimetry was performed to study the surface adsorptive properties.

MATERIALS AND METHODS

Materials

Diatomite silica and kaolin were obtained from the Nasarawa and Ekiti States of Nigeria, respectively. The samples were dried at 105°C for 2 h, and then cooled to room temperature for further treatment. Analytical-grade nitric acid (30% HNO_3) was selected for acid leaching and activation. Analytical-grade silver nitrate ($AgNO_3$), sodium carbonate (Na_2CO_3) and titanium dioxide (TiO_2) were used to prepare Ag-TiO_2 photocatalyst NPs *via* intercalation into the materials' microstructures.

Chemical modification

Acid-treated kaolin (denoted as KLN) and diatomite (denoted as ZEO) were prepared from their raw materials. Acid treatment removed the fine impurities and carbonaceous materials, increasing the number of active sites on the crystallite surfaces and opening more pores in the microstructure for intercalation of photocatalyst Ag-TiO_2 NPs (Fig. 1). Using the sol–gel technique, dispersions of modified Ag-TiO_2 NPs (STOX) were prepared according to Ajenifuja *et al.* (2017a, 2017b). For intercalation, 25 g of activated kaolin or diatomite were added slowly into the continuously stirred Ag-TiO_2 colloidal solution (~10 g in 100 mL ethanol), and the slurry was stirred and mildly heated for 2 h on a hot plate. The intercalated Ag-TiO_2-kaolin and Ag-TiO_2-diatomite photocatalyst nanocomposites (denoted as STOX-K and STOX-Z, respectively) were recovered from the colloidal suspension *via* centrifugation and subsequent drying. Colour change from off-white to purplish-white was observed before sintering. The ceramic powders were further sintered at temperatures ranging between 900°C and 1000°C for 12 h for thermal fusion and densification of the constituents, and the final products were designated as STOX-KS and STOX-ZS, respectively.

Physical and chemical characterization

The specific surface areas of KLN and ZEO, photocatalyst nanocomposite materials (STOX-K and

https://doi.org/10.1180/clm.2018.50 Published online by Cambridge University Press

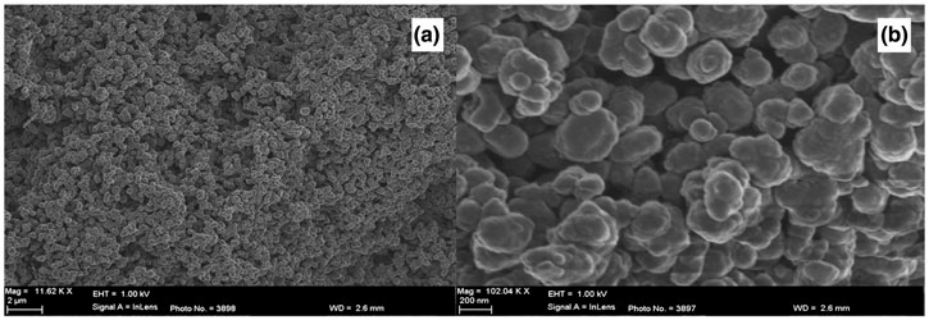

FIG. 1. SEM images showing the morphology of the NPs of Ag-TiO_2 (STOX) at (a) low and (b) high magnifications.

STOX-Z) and sintered samples (STOX-KS and STOX-ZS) were obtained by nitrogen adsorption–desorption isotherms at 77.350°K and an ambient temperature of 22.0°C using a BET analyser (TriStar II 3020 version 2.00). Thermal characterization was performed with DSC (NETZSCH 404 PC). The surface and microstructural changes in the samples were studied with SEM (ZEISS DSM-940A) on carbon-coated samples. Elemental characterization of the samples before and after intercalation of the photocatalyst was performed by EDX. The elemental compositions of the acid-treated and intercalated minerals are listed in Table 1.

RESULTS AND DISCUSSION

Microstructural analysis

The sol–gel-prepared Ag-TiO_2 consists of evenly distributed networks of NPs of uniform size (Fig. 1). Each particle is an aggregate of smaller Ag-TiO_2 particles (Fig. 1b). The micrographs of kaolin-based samples (KLN, STOX-K and STOX-KS) display changes in the microstructure after modification (Fig. 2). Dispersed crystallites of the Ag-TiO_2-kaolin nanocomposite with well-defined grain surfaces are observed in the sintered STOX-KS sample, while the acid-treated sample KLN is largely composed of particle aggregates interspersed with compact masses of particles or grains. The unsintered intercalated nanocomposite STOX-K is microstructurally identical to KLN with larger aggregations of particles. Figure 3 shows the SEM images of diatomite-based ceramic photocatalysts. The Ag-TiO_2 NPs are dispersed within the pores and channels, while some NPs attach to pores and mineral surfaces in sample STOX-Z. Comparing the sintered and unsintered diatomite photocatalyst nanocomposites, the original pore structure evolves into a zeolite-like homogeneous crystal structure (Fig. 3c). The notable morphological changes between ZEO and STOX-ZS ceramic particles indicate that the chemical and thermal processes successively decomposed the original structure of the diatomaceous material, forming a microstructure with various textural characteristics. Due to the heating, TiO_2 NPs are now interspersed into and on the surface of the pores. The micrographs of sintered photocatalyst–mineral nanocomposites even show aggregation of particles of well-defined surface microstructures (Figs 2c, 3c). With increasing sintering temperature, the SiO_2 catalyst is better crystallized and the number of defect sites is reduced, thereby enhancing photocatalytic activity (Wang *et al.*, 2009).

TABLE 1. EDX analysis of activated and intercalated natural materials. C is present due to the carbon coating of the samples.

Element	Concentration (wt.%)			
	KLN	STOX-K	ZEO	STOX-Z
C	6.22	5.93	19.10	9.19
O	57.27	51.61	55.51	55.10
Al	18.39	15.90	1.43	1.09
Si	17.99	15.80	23.27	21.25
Ca	–	1.16	0.22	0.35
Fe	–	–	0.49	0.68
Ti	–	9.33	–	12.33
Na	0.13	0.23	–	–

Physisorption hysteresis analysis

The N_2-adsorption isotherm analysis is based on the International Union of Pure and Applied Chemistry (IUPAC) classification (Sing *et al.*, 1985). The isotherms of the treated materials and modified

https://doi.org/10.1180/clm.2018.50 Published online by Cambridge University Press

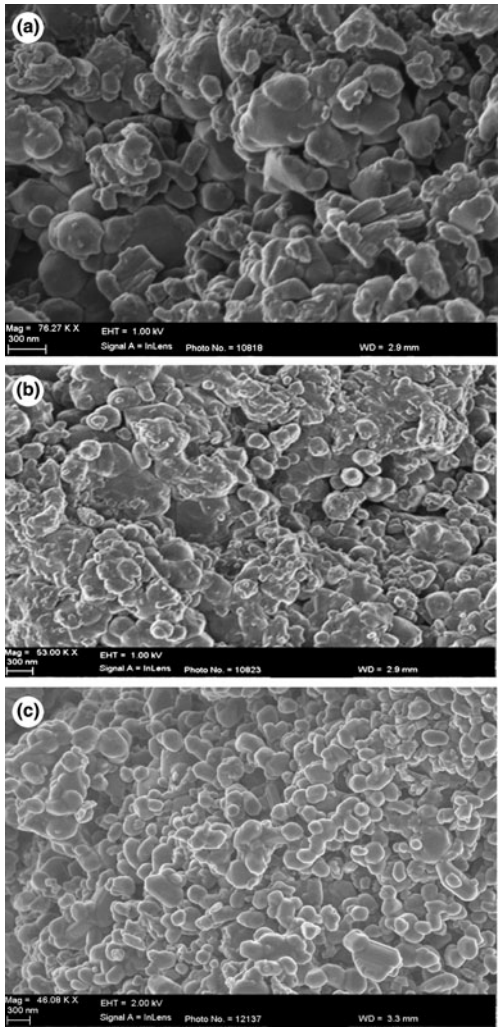

FIG. 2. SEM images of the modified kaolin materials. (a) KLN sample showing aggregated lumpy and rod-like microstructures. (b) STOX-K sample intercalated with Ag-TiO_2 prepared by the sol–gel technique. (c) STOX-KS with refined particulate surface morphology.

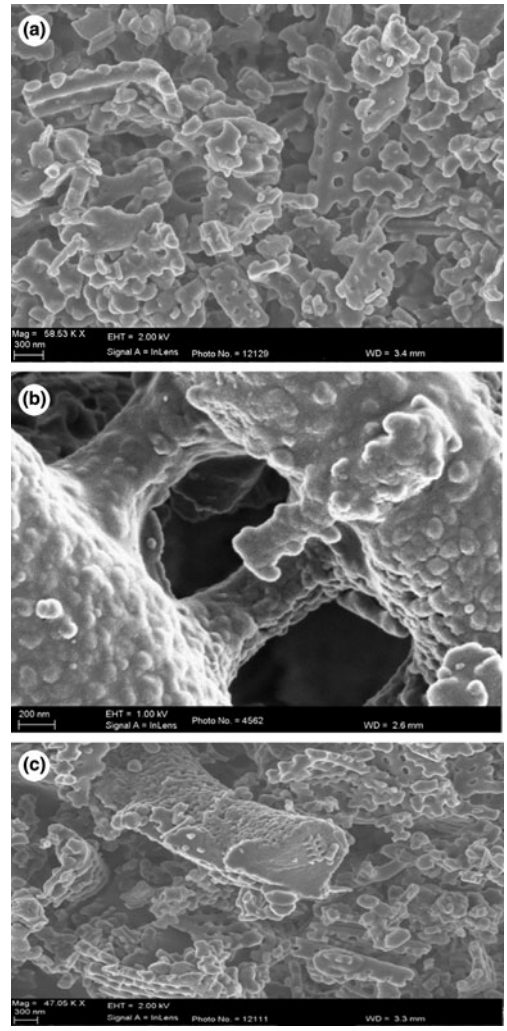

FIG. 3. SEM images of the modified kaolin materials. (a) Natural pores of the ZEO sample after treatment with HNO_3. (b) STOX- Z sample intercalated with Ag-TiO_2 prepared by the sol–gel technique. (c) Sintered intercalated sample STOX-ZS.

nanocomposite samples are shown in Figs 4 and 5 for samples KLN and ZEO, respectively. The original and modified materials display type III isotherms and H3 hysteresis loops. This indicates the presence of mesopores in the materials and an unrestricted multilayer formation, because the lateral interactions between adsorbed molecules are strong in comparison to interactions between the adsorbent and adsorbate. The H3 hysteresis loops are often caused by adsorption of non-polar gases on loose assemblages of plate-like particles, forming slit-pores. The shape of the hysteresis loops shows the non-rigid nature of the treated mineral (KLN/ZEO) and nanocomposite (STOX-K/STOX-Z) microstructures (Figs 4, 5). In addition, the sintered nanocomposites have distinct hysteresis loops (Figs 4, 5).

The isotherm for the acid-treated kaolin sample (KLN) exhibits real hysteresis between adsorption and desorption branches, with the gap decreasing slightly in the Ag-TiO_2-intercalated sample STOX-K. In the

https://doi.org/10.1180/clm.2018.50 Published online by Cambridge University Press

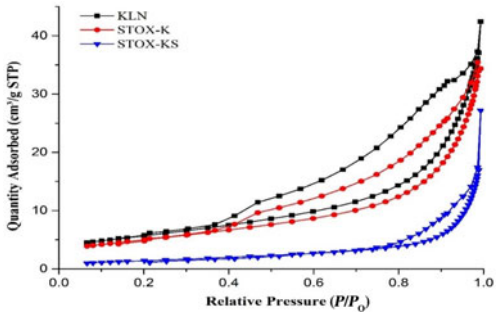

FIG. 4. Nitrogen adsorption/desorption isotherms for samples KLN, STOX-K and STOX-KS. STP = standard temperature and pressure.

sintered nanocomposite (STOX-KS), the hysteresis loop decreases further, with closure point at $P/P_0 \sim 0.8$, suggesting a greater number of macropores in grain boundaries in sintered photocatalyst nanocomposites. It follows that the adsorption type changes from chemical (chemisorption) to physical (physisorption). Before intercalation, the acid treatment improved the pore, surface and particle-size distributions of the materials (Samyn *et al.*, 2015). Moreover, adsorption is irreversible in chemisorption, while it is reversible in physisorption, with adsorption and desorption processes following a common path (Rouquerol *et al.*, 1999). Reversible sorption is desirable in the recovery or recycling of the adsorbents for later use. Samples KLN and STOX-K display type II isotherms at lower P/P_0 values, with monolayer adsorption in the mesopores. Because the shape of the isotherm is partly dependent on the texture of the porous materials, chemical and thermal treatments induced microstructural changes in the materials.

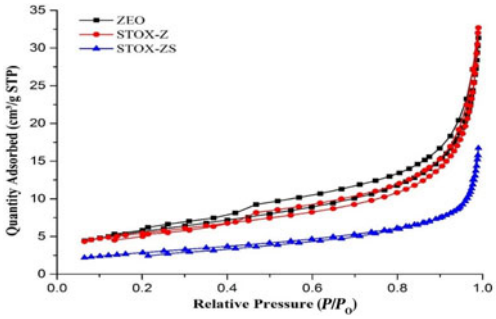

FIG. 5. Nitrogen adsorption/desorption isotherms for samples ZEO, STOX-Z and STOX-ZS. STP = standard temperature and pressure.

The Ag-TiO_2-diatomite photocatalyst nanocomposite samples (Fig. 5) display hysteresis loops and isotherms that are comparable to those of the kaolin samples (type H3 and type III, respectively), except for the smaller hysteresis between adsorption and desorption branches. The steep increase in N_2 gas adsorption at intermediate relative pressures ($P/P_0 = 0.3–0.6$) for the ZEO and STOX-Z samples may be attributed to the presence of mesopores of uniform size (Li *et al.*, 2013). The increase in adsorption at high P/P_0 values corresponds to the activities of the macropores formed by agglomeration of the inherent mesoporous particles. In addition, the almost horizontal isotherm of the sintered STOX-KS sample at low relative pressure suggests the presence of narrow-slit pores in the micropore regions and multilayer formation with strong interaction between the adsorbed molecules (Kruk & Jaroniec, 2001).

After intercalation and sintering, the adsorption–desorption isotherm of ZEO became totally reversible, indicating changes in the adsorbate–adsorbent interactions of the photocatalyst nanocomposites with the adherence of Ag-TiO_2 NPs on their surface. Generally, the specific surface area decreased mainly due to inter- and intra-particle densification, which increased average grain size (Burg *et al.*, 2007; Bakhsh *et al.*, 2014), and the pore size increased from the annihilation of micropores within the microstructure after intercalation and sintering (Table 2). In all of the samples, the first few multilayers of the adsorbate gas seem to form before transition to the relatively high-pressure region, where hysteresis characteristics depend on the chemical treatments and intercalation of the photocatalysts.

Previous experimental studies (Ajenifuja *et al.*, 2017a, 2017b) showed that the sintered nanocomposites exhibited greater degradation capacities and adsorption capacities for concentrated Cu^{2+} and Co^{2+} aqueous solutions (100–1000 mg/L). This is in agreement with previous studies on the effects of sintering temperature on the performance of photocatalyst–silica composites on the degradation of pollutants in aqueous suspensions (Du *et al.*, 2008; Wang *et al.*, 2009). With increasing sintering temperature, the crystallization of the catalyst–silica is enhanced and the number of defect sites is reduced (Hoffmann *et al.*, 1995; Carp *et al.*, 2004). In addition, the intercalation of photocatalyst NPs in silica and aluminosilicate microstructures involves dispersion on the surface of these phases and retards grain growth within the NPs during sintering, which may diminish their activity due to the reduced specific surface area (Caratto *et al.*, 2013). Therefore, photocatalyst

https://doi.org/10.1180/clm.2018.50 Published online by Cambridge University Press

TABLE 2. Specific surface area and porosity parameters for kaolin clay adsorbents.

Samples	Specific surface area (m^2/g)		Pore volume (cm^3/g)		Pore size (Å)	
	S_{BET}	$S_{t\text{-MICRO}}$	$V_{Total(SP)}$	$V_{t\text{-MICRO}}$	D_{BET}	D_{BJH}
KLN	20.24	1.0114	0.055396	0.000380	109.4561	115.002
STOX-K	18.06	21.176	0.049650	−0.000176	109.9514	104.889
STOX-KS	5.45	7.433	0.023837	−0.000720	175.0815	226.777
ZEO	19.58	0.7929	0.042170	0.000511	86.1411	90.137
STOX-Z	18.40	2.6037	0.042843	0.001499	93.1544	103.536
STOX-ZS	10.15	11.828	0.021176	−0.000173	83.4675	89.428

crystallites supported on SiO_2 substrates have smaller average particle sizes than those of the unsupported photocatalysts.

Surface and porosimetry analysis

Pure catalyst NPs might display lower degradation efficiencies due to self-aggregation (Caratto *et al.*, 2013). However, intercalation of NPs into platelets and attachment on porous scaffolds or substrates affects their porosity while simultaneously enhancing the inherent surface properties of the composite. The physical parameters of the treated and nanocomposite samples are shown in Table 2. The acid-treated samples KLN and ZEO have relatively high specific surface areas (S_{BET} = 20.24 and 19.58 m^2/g, respectively) compared to the sintered intercalated samples. The specific surface area of natural diatomite is ∼3.81 ± 0.1 m^2/g (Tsai *et al.*, 2006); hence, acid treatment opened more pores and reduced the grain size of mineral particles. After intercalation and sintering, and due to the anchoring of the catalyst NPs on the silica substrates, the specific surface area of the nanocomposite material decreases remarkably, especially after sintering (S_{BET} = 5.45 and 10.15 m^2/g for the STOX-KS and ZTOX-ZS, respectively). This might be attributed to the increase in crystallite size due to grain growth and photocatalyst NP precipitation on silica particles during sintering. Grain growth occurs when recovery and recrystallization are complete within the material. Because treated aluminosilicate boundaries are areas of high energy, they make excellent sites for the nucleation of photocatalyst NPs and other secondary phases. After sintering, remarkable reduction in the surface area was observed as a result of a reduction in the actual number of grains per volume of the nanocomposite (Hubbard, 2002; Ratke & Voorhees, 2002).

Another effect of sintering on homogeneous or composite materials is densification, which reduces total porosity. Although the pore size of photocatalyst–diatomite nanocomposites reduced slightly after sintering, the pore size of photocatalyst–kaolin composites increased significantly. This difference is attributed to the various microstructural properties of the materials. Diatomites are inherently microporous materials with well-defined channels and pores, but kaolins are mainly porous at the grain boundaries and within the kaolinite platelets. The photocatalyst NPs in sample STOX-ZS are distributed evenly on the surface and in the pore channels of the diatomite microstructure, thereby reducing the pore diameter (Fig. 3c). The larger pores observed on the sintered kaolin nanocomposite are mainly located at grain boundaries and between the kaolinite layers. Because the treated kaolin was heated to >1050°C during sintering, the adjacent spinel phase might have nucleated and transformed into mullite and cristobalite (Tomura *et al.*, 1985; Deer *et al.*, 1994; Bellotto *et al.*, 1995; Huertas *et al.*, 1999). In spite of the increase in the pore size for sintered kaolin nanocomposites, the pore volume was relatively low, which is probably due to the densification and grain growth induced by sintering. Modification of photocatalyst NPs anchored on suitable mineral substrates rather than the use of pure NPs has been well established in previous studies (Kay *et al.*, 2006; Wang *et al.*, 2009). It reduces costs significantly, because the materials are naturally available and abundant and there is no subsequent effect on the environment.

Thermal analysis

The DSC curves of photocatalyst TiO_2 (TOX) and STOX NPs are shown in Fig. 6. Both TiO_2-based samples exhibited initial endothermic reactions at

https://doi.org/10.1180/clm.2018.50 Published online by Cambridge University Press

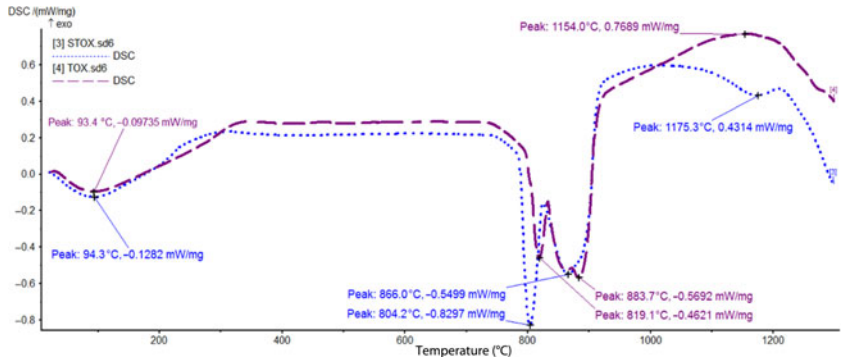

FIG. 6. DSC thermograms showing thermal transformations of samples TOX and STOX.

93.4°C and 94.3°C, respectively, which might be attributed to the release of adsorbed water. Further heating led to dual endothermic events at 804.2°C and 866.0°C (STOX) and 819.1°C and 883.7°C (TOX). The endothermic events are attributed to a successive phase transition and recrystallization of the TiO_2 NPs. The left-shift of the dual endothermic events for STOX might be attributed to the influence of Ag-NPs on the TiO_2 NPs. Metastable anatase and brookite TiO_2 phases usually convert irreversibly to the stable rutile phase upon heating to >600–800°C (Greenwood & Earnshaw, 1984). The broad exothermic peak at 1154°C in pure TOX samples is attributed to phase recrystallization by solid-state reaction encouraged by oxidation and grain growth by Ostwald ripening. Moreover, at 1175.3°C, an endothermic peak was observed for STOX samples, in contrast to the exothermic reaction observed in TOX samples at that temperature. This could be ascribed to the phase transformation due to melting of the doping silver NPs in the TiO_2 matrix.

The DSC curves obtained for the acid-treated mineral particles exhibit both exothermic and endothermic events, and transformations are shown in Figs 6–8. Owing to the open-frame structure in geological minerals, water molecules are often trapped in their frameworks. The various thermal behaviours of the acid-treated diatomite (ZEO) and photocatalyst nanocomposite sample (STOX-Z) are depicted in Fig. 8. Endothermic and exothermic transformations are observed for the Ag-TiO_2-diatomite nanocomposite at 762.3°C and 1153.9°C, respectively. An exothermic event attributed to recrystallization is also detected in sample ZEO at 1172.7°C. The events at low temperatures (103.6°C and 110.6°C) are ascribed to the removal or desorption of adsorbed water. Recrystallization of TiO_2 NPs in the Si-rich microstructure into rutile is indicated by the endothermic peak at 762.3°C. For the acid-treated kaolin (KLN) and intercalated nanocomposite (STOX-K), low-temperature endothermic peaks were also observed at 131.9°C and 121.8°C, closely followed by a set of related

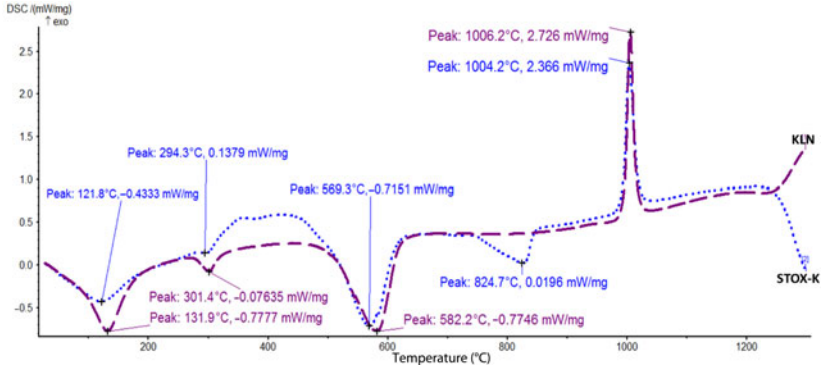

FIG. 7. DSC thermograms showing thermal transformations of samples KLN and STOX-K.

https://doi.org/10.1180/clm.2018.50 Published online by Cambridge University Press

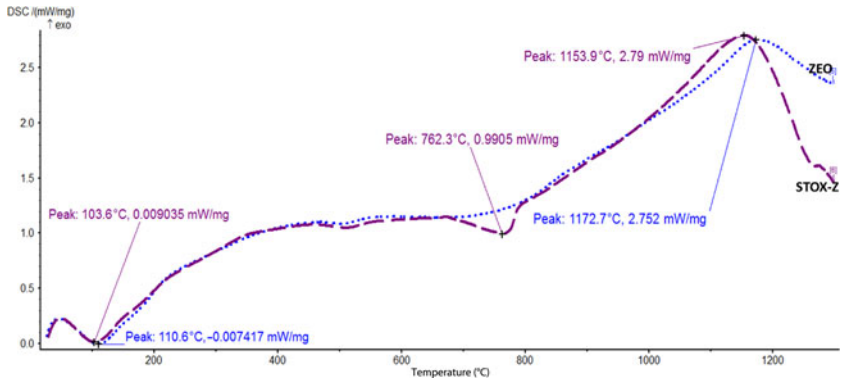

FIG. 8. DSC thermograms showing thermal transformations of samples ZEO and STOX-Z.

endothermic peaks at 294.3°C and 301.4°C (Fig. 7). The endothermic peaks in Fig. 7 are shifted to lower temperatures in the photocatalyst nanocomposite due to photocatalyst intercalation. The intense, well-defined endotherms observed between 500°C and 600°C for both materials are attributed to the dehydroxylation of kaolinite to form disordered metakaolin (Bellotto *et al.*, 1995). The thermal reaction observed in sample STOX-Z is also exhibited by STOX-K at 824.7°C. Finally, the sharp exothermic events at ∼1004.2°C and ∼1006.2°C for STOX-K and STOX-KS, respectively, signify nucleation of secondary phases and recrystallization of spinel phases into mullite and cristobalite.

CONCLUSION

Photocatalyst nanocomposite materials were prepared from Ag-TiO_2 NPs and locally available kaolin and diatomite. Intercalation and relatively high-temperature sintering processes induced remarkable changes into the physical and chemical properties of the original materials. The changes indicated that kaolin and diatomite are suitable as photocatalyst composite and support materials for Ag-TiO_2 NPs. The treated and nanocomposite samples showed multilayer N_2 adsorption at low relative pressure (<0.4), while sintered samples are active at high P/P_0 (>0.6). Adsorption and desorption processes followed common paths in the BET analysis of the sintered nanocomposite samples, as was indicated by the reversible isotherms and a change from chemisorption to physisorption with sintering. Physisorption processes are highly desirable for material recovery after the degradation and removal of pollutants. Additionally, high-hysteresis closure points ($P/P_0 \sim 0.8$) indicate rigid pore structures and stable microstructural surfaces after sintering. Recrystallization of the material–photocatalyst nanocomposite by sintering improved the surface adhesion of the photocatalyst on the minerals.

ACKNOWLEDGEMENTS

The support of The World Academy of Science (TWAS) in collaboration with the National Research Foundation (NRF) towards this research is hereby acknowledged.

REFERENCES

Ajenifuja E., Ajao J.A. & Ajayi E.O. (2017a) Adsorption isotherm studies of Cu (II) and Co (II) in high concentration aqueous solutions on photocatalytically modified diatomaceous ceramic adsorbents. *Applied Water Science*, **7**, 3793–3801.

Ajenifuja E., Ajao J.A. & Ajayi E.O. (2017b) Equilibrium adsorption isotherm studies of Cu (II) and Co (II) in high concentration aqueous solutions on Ag-TiO_2-modified kaolinite ceramic adsorbents. *Applied Water Science*, **7**, 2279–2286.

Alexandre M. & Dubois P. (2000) Polymer-layered silicate nanocomposites: preparation, properties and uses of a new class of materials. *Materials Science Engineering*, **28**, 1–63.

Bakhsh N., Khalid F.A. & Hakeem A.S. (2014) Effect of sintering temperature on densification and mechanical properties of pressureless sintered CNT–alumina nanocomposites. *IOP Conference Series: Materials Science and Engineering*, **60**, 012059.

Bellotto M., Gualtieri A., Artioli G. & Clark S.M. (1995) Kinetic study of the kaolinite-mullite reaction sequence. Part I: kaolinite dehydroxylation. *Physics and Chemistry of Minerals*, **22**, 207–214.

https://doi.org/10.1180/clm.2018.50 Published online by Cambridge University Press

Bergaya F., Theng B.K. & Lagaly G. (2006) *Handbook of Clay Science* (1st edition). Elsevier, Amsterdam, The Netherlands.

Burg T., Bak T., Nowotny J., Sheppard L., Sorrell C.C. & Vance E.R. (2007) Effect of sintering on microstructure of TiO_2 ceramics. *Advances in Applied Ceramics*, **106**, 57–62.

Caratto V., Aliakbarian B., Casazza A.A., Setti L., Bernini C., Perego P. & Ferretti M. (2013) Inactivation of Escherichia coli on anatase and rutile nanoparticles using UV and fluorescent light. *Materials Research Bulletin*, **48**, 2095–2101.

Carp O., Huisman C.L. & Reller A. (2004) Photoinduced reactivity of titanium dioxide. *Progress in Solid State Chemistry*, **32**, 133–177.

Carrado K.A. (2004) Introduction: clay structure, surface acidity, and catalysis. Pp. 1–38 in: *Handbook of Layered Materials, Part I* (S. Auerbach, K.A. Carrado & P.K. Dutta, editors). Marcel Dekker, New York, NY, USA.

Chong M.N., Tneu Z.Y., Poh P.E., Jin B. & Aryal R. (2014) Synthesis, characterisation and application of TiO_2–zeolite nanocomposites for the advanced treatment of industrial dye wastewater. *Journal of the Taiwan Institute of Chemical Engineers*, **2014**, 1–9.

Deer W.A., Howie R.A. & Zussman J. (1994) *An Introduction to the Rock-Forming Minerals*. Longman, Harlow, UK.

Defontaine G., Barichard A., Letaief S., Feng C., Matsuura T. & Detellier C. (2010) Nanoporous polymer–clay hybrid membranes for gas separation. *Journal of Colloid and Interface Science*, **343**, 622–627.

Du W., Xu Y. & Wang Y. (2008) Photoinduced degradation of orange II on different iron (hydr) oxides in aqueous suspension: rate enhancement on addition of hydrogen peroxide, silver nitrate, and sodium fluoride. *Langmuir*, **24**, 175–181.

Elbokl T.A. & Detellier C. (2006) Aluminosilicate nanohybrid materials. Intercalation of polystyrene in kaolinite. *Journal of the Physics and Chemistry of Solids*, **67**, 950–955.

Elbokl T.A. & Detellier C. (2009) Kaolinite-poly(methacrylamide) intercalated nanocomposite *via in situ* polymerization. *Canadian Journal of Chemistry*, **87**, 272–279.

Faulde M.K., Tisch M. & Scharninghausen J.J. (2006) Efficacy of modified diatomaceous earth on different cockroach species (Orthoptera, Blattellidae) and silverfish (Thysanura, Lepismatidae). *Journal of Pest Science*, **79**, 155–161.

Fernandez-Saavedra R., Darder M., Gomez-Aviles A., Aranda P. & Ruiz-Hitzky E. (2008) Polymer–clay nanocomposites as precursors of nano structured carbon materials for electrochemical devices: templating effect of clays. *Journal of Nanoscience and Nanotechnology*, **8**, 1741–1750.

Ferraz E., Coroado J., Silva J., Gomes C. & Rocha F. (2011) Manufacture of ceramic bricks using recycled brewing spent kieselguhr. *Materials and Manufacturing Processes*, **26**, 1319–1329.

Fields P., Allen S., Korunic Z., McLaughlin A. & Stathers T. (2002) Standardized testing for diatomaceous earth. Pp. 779–784 in: *Proceedings of the Eighth International Working Conference of Stored-Product Protection, York, UK*. EurekaMag, York, UK.

Gómez-Romero P. & Sanchez C. (2004) *Functional Hybrid Materials*. Wiley-VCH, Weinheim, Germany.

Greenwood N.N. & Earnshaw A. (1984) *Chemistry of the Elements*. Pergamon Press, Oxford, UK.

Hathway T. & Jenks W.S. (2008) Effects of sintering of TiO_2 particles on the mechanisms of photocatalytic degradation of organic molecules in water. *Journal of Photochemistry and Photobiology A: Chemistry*, **200**, 216–224.

Hoffmann M.R., Martin S.T., Choi W. & Bahnemann D. W. (1995) Environmental applications of semiconductor photocatalysis. *Chemistry Reviews*, **95**, 69–96.

Hubbard A.T. (2002). *Encyclopedia of Surface and Colloid Science*. Taylor & Francis, Abingdon, UK.

Huertas F.J., Fiore S., Huertas F. & Linares J. (1999) Experimental study of the hydrothermal formation of kaolinite. *Chemical Geology*, **156**, 171–190.

Jiang W., Mashayekhi H. & Xing B. (2009) Bacterial toxicity comparison between nano and micro-scaled oxide particles. *Environmental Pollution*, **157**, 1619–1625.

Kay A., Cesar I. & Grätzel M. (2006) New benchmark for water photooxidation by nanostructured alpha-Fe_2O_3 films. *Journal of the American Chemical Society*, **128**, 15714–15721.

Komadel P. (1999) Structure and chemical characteristics of modified clays. Pp. 3–18 in: *Natural Microporous Materials in Environmental Technology* (P. Misaelides, F. Macasek, T.J. Pinnavaia & C. Collela, editors). Kluwer Academic, Dordrecht, The Netherlands.

Kruk M. & Jaroniec M. (2001) Gas adsorption characterization of ordered organic–inorganic nanocomposite materials. *Chemistry of Materials*, **13**, 3169–3183.

Leiviskä T., Gehör S., Eijärvi E., Sarpola A. & Tanskanen J. (2012) Characteristics and potential applications of coarse clay fractions from Puolanka, Finland. *Central European Journal of Engineering*, **2**, 239–247.

Letaief S., Aranda P., Fernandez-Saavedra R., Margeson J.C., Detellier C. & Ruiz-Hitzky E. (2008) Poly(3, 4-ethylenedioxythiophene)–clay nanocomposites. *Journal of Materials Chemistry*, **18**, 2227–2233.

Li S.Q., Zhu R.R., Zhu H., Xue M., Sun X.Y., Yao S.D. & Wang S.L. (2008) Nanotoxicity of TiO_2 nanoparticles to erythrocyte *in vitro*. *Food Chemistry and Toxicology*, **46**, 3626–3631.

Li S., Wu Q., Cui C., Lu G., Zhang C. & Yan Z. (2013) Preparation of TiO_2/Al–MCM-41 mesoporous

https://doi.org/10.1180/clm.2018.50 Published online by Cambridge University Press

materials from coal-series kaolin and photodegradation of methyl orange. *Materials Science – Poland*, **31**, 372–377.

Mokaya R., Jones W., Davies M.E. & Whittle M.E. (1993) Preparation of alumina-pillared acid-activated clays and their use as chlorophyll adsorbents. *Journal of Materials Chemistry*, **3**, 381–387.

Ozcan A.S. & Ozcan A. (2004) Adsorption of acid dyes from aqueous solutions onto acid-activated bentonite. *Journal of Colloid and Interface Science*, **276**, 39–46.

Pinnavaia T.J. & Beall G.W. (2000) *Polymer–Clay Nanocomposites*. Wiley, Oxford, UK.

Plachá D., Martynková G.S. & Rümmeli M.H. (2008) Preparation of organovermiculites using HDTMA: structure and sorptive properties using naphthalene. *Journal of Colloid and Interface Science*, **327**, 341–347.

Plachá D., Rosenbergová K., Slabotínsky J., Kutláková K. M., Studentová S. & Martynková G.S. (2014) Modified clay minerals efficiency against chemical and biological warfare agents for civil human protection. *Journal of Hazardous Materials*, **271**, 65–72.

Ratke L. & Voorhees P.W. (2002) *Growth and Coarsening: Ostwald Ripening in Material Processing*. Springer Science & Business Media, Berlin, Germany.

Ray S. & Okamoto M. (2003) Polymer/layered silicate nanocomposites: a review from preparation to processing. *Progress in Polymer Science*, **28**, 1539–1541.

Rouquerol F., Rouquerol J. & Sing K. (1999) *Adsorption by Powders and Porous Solids*. Academic Press, London, UK.

Ruiz-Hitzky E. & Van Meerbek A. (2006) Polymer–clay nanocomposites. Pp. 113–142 in: *Handbook of Clay Science* (F. Bergaya, B. Theng & G. Lagaly, editors). Elsevier, Amsterdam, The Netherlands.

Samyn P., Schoukens G., & Stanssens D. (2015) Kaolinite nanocomposite platelets synthesized by intercalation and imidization of poly(styrene-co-maleic anhydride). *Materials*, **8**, 4363–4388.

Sing K.S., Everett D.H., Haul R.A., Moscou L., Pierotti R. A., Rouquerol J. & Siemieniewska T. (1985) Physical and biophysical chemistry division commission on colloid and surface chemistry including catalysis. *Pure and Applied Chemistry*, **57**, 603–619.

Szabó T., Németh J. & Dékány I. (2003) Zinc oxide nanoparticles incorporated in ultrathin layer silicate films and their photocatalytic properties. *Colloids and Surfaces A*, **230**, 23–35.

Tomura S., Shibasaki Y., Mizuta H. & Kitamura M. (1985) Growth conditions and genesis of spherical and platy kaolinite. *Clays and Clay Minerals*, **33**, 200–206.

Tsai W.-T., Lai C.-W. & Hsien K.-J. (2006) Characterization and adsorption properties of diatomaceous earth modified by hydrofluoric acid etching. *Journal of Colloid and Interface Science*, **297**, 749–754.

Tunney J.J. & Detellier C. (1996) Aluminosilicate nanocomposite materials: poly(ethylene glycol)–kaolinite intercalates. *Chemistry of Materials*, **8**, 927–935.

Vicente Rodriguez M.A., Suarez Barrios M., Lopez Gonzalez J.D. & Banares Munoz M.A. (1994) Acid activation of a ferrous saponite (griffithite): physicochemical characterization and surface area of the products obtained. *Clays and Clay Minerals*, **42**, 724–730.

Vimonses V., Chong M.N. & Jin B. (2010) Evaluation of the physical properties and photodegradation ability of titania nanocrystalline impregnated onto modified kaolin. *Microporous Mesoporous Materials*, **132**, 201–209.

Wang Y., Du W. & Xu Y. (2009) Effect of sintering temperature on the photocatalytic activities and stabilities of hematite and silica-dispersed hematite particles for organic degradation in aqueous suspensions. *Langmuir*, **25**, 2895–2899.

Warheit D.B., Hoke R.A., Finlay C., Maria Donner E., Reed K.L. & Sayes C.M. (2007) Development of a base set of toxicity tests using ultrafine TiO_2 particles as a component of nanoparticle risk management. *Toxicology Letters*, **171**, 99–110.

https://doi.org/10.1180/clm.2018.50 Published online by Cambridge University Press